

# RSC Advances



This is an *Accepted Manuscript*, which has been through the Royal Society of Chemistry peer review process and has been accepted for publication.

*Accepted Manuscripts* are published online shortly after acceptance, before technical editing, formatting and proof reading. Using this free service, authors can make their results available to the community, in citable form, before we publish the edited article. This *Accepted Manuscript* will be replaced by the edited, formatted and paginated article as soon as this is available.

You can find more information about *Accepted Manuscripts* in the [Information for Authors](#).

Please note that technical editing may introduce minor changes to the text and/or graphics, which may alter content. The journal's standard [Terms & Conditions](#) and the [Ethical guidelines](#) still apply. In no event shall the Royal Society of Chemistry be held responsible for any errors or omissions in this *Accepted Manuscript* or any consequences arising from the use of any information it contains.

## Polyaniline nanofibers-graphene oxide nanoplatelets composite thin film electrodes for electrochemical capacitors

Mohd. Khalid<sup>a\*</sup>, Milton A. Tumelero<sup>a</sup>, Vinicius C. Zoldan<sup>a</sup>, Cristiani C. Pla Cid<sup>a</sup>, Dante F. Franceschini<sup>b</sup>, Ronaldo A. Timm<sup>c</sup>, Lauro T. Kubota<sup>c</sup>, Stanislav A. Moshkalev<sup>d</sup>, Andre A. Pasa<sup>a\*</sup>

<sup>a</sup> *Laboratório de Filmes Finos e Superfícies, Departamento de Física, Universidade Federal de Santa Catarina 88040-900-Florianopolis, Brazil*

<sup>b</sup> *Instituto de Física, Universidade Federal Fluminense, Niterói-RJ, Brazil*

<sup>c</sup> *Departamento Química Analítica, IQ-UNICAMP, Campinas, SP, Brazil*

<sup>d</sup> *Center for Semiconductor Components, State University of Campinas, Campinas, SP, Brazil*

\* Corresponding authors. Tel.: +55 4884061547. E-mail address: [mkansarister@gmail.com](mailto:mkansarister@gmail.com) (M. Khalid), [andre.pasa@ufsc.br](mailto:andre.pasa@ufsc.br) (A.A. Pasa).

### Abstract:

Composite thin films of polyaniline (PANI) nanofibers and graphene oxide (GO) nanoplatelets are synthesized through an easy electrodeposition process for electrochemical capacitors. The morphology and structure of the materials are investigated by field emission scanning electron microscopy, transmission electron microscopy, current sensing atomic force microscopy, X-ray photoelectron spectroscopy, Fourier transforms infrared spectroscopy, X-ray diffraction, and ultraviolet-visible spectroscopy. In the process of electrodeposition, the electrostatic interactions between the oxygen functionalized graphene and aniline monomers at an electrolyte interface assisted the co-deposition of PANI nanofibers and GO nanoplatelets. These thin films have an excellent effect on the electrochemical properties with an electrochemical capacitance of 662 F g<sup>-1</sup> at low current density of 0.025 mA cm<sup>-2</sup> simultaneously with high energy density (64.5 Wh kg<sup>-1</sup>) and high power density (1159 W kg<sup>-1</sup>). The excellent electrochemical performance of the films is attributed to the unique structure of the material, showing synergy between PANI nanofibers and GO nanoplatelets.

## 1. Introduction

The development of alternative energy resources with elevated energy and high power density has received noteworthy attention since the end of the last century due to the depletion of fossil fuels and global warming [1-3]. Thin film electrochemical capacitors are the most promising energy sources that can meet these demands. Electrochemical capacitors are also known as supercapacitors provide high power density than batteries and high energy density than conventional capacitors. Despite these advantages, supercapacitors have low energy density than batteries and an enhancement in the energy density remains a great challenge in supercapacitor research. Nowadays, much research on electrochemical capacitors has aimed to achieve high specific capacitance with simultaneously high energy density and high power density at low production cost [4, 5]. Based on the charge storage mechanism, electrochemical devices could be divided into electrochemical double layer capacitors and pseudocapacitors, in which energies are stored in the form of electric double layer at the interface of electrode/electrolyte, and reversible redox reactions of the electroactive species, respectively. Conductive carbon based materials are usually adopted as electrode materials for storing the charge through electrochemical double layer and can exhibit high power densities, because faster ion flow than redox reactions. On the other hand, conducting polymers and metal oxides are usually used as pseudocapacitors electrode materials, which store energy through electrochemical reactions and can exhibit high energy densities.

The synthesis and design of conducting polymers with carbon materials are important for the development of nanocomposite thin films, which can enable large area, and low cost electrode material to be constructed. Among the conducting polymers, PANI is regarded as one of the most promising materials due to its excellent conductivity, high electrochemical activity, stability in air and water, low cost, and ease of synthesis [6]. Although the application of PANI as supercapacitor material is rather limited due to its poor processing performance and cyclic stability. Therefore, it is often hybridized with carbon materials to prepare a composite and used in supercapacitors with better specific capacitance and mechanical stability [7-10]. Recently, graphene oxide has attracted substantial interest as a promising precursor for preparing graphene based composite materials. GO is the oxidized form of graphene and its structure can be visualized as a graphene sheet with its basal plane and edges decorated by oxygen-containing

groups [11-13]. It has been demonstrated that the presence of oxygen-containing functional groups on graphene facilitate the surface modification for making composite with conducting polymers. Recently, researchers have reported the synergistic combination of GO with conjugated polymers and their dramatic improvements in electrochemical properties [14-18]. Interestingly, GO has shown the excellent capacitance and good cycle durability than graphene [19, 20]. Numerous methods have been explored to design new structure materials of PANI and graphene, the most of literature follows the simple solution mixing, *in-situ* polymerization, and electropolymerization of aniline in the presence of GO or reduced GO [21-28]. Xu *et al.* [29] have demonstrated the hierarchical composites of polyaniline nanowires arrays on graphene oxides through a chemical method, which shows a high specific capacitance of 555 F g<sup>-1</sup> at a discharge current density of 0.2 A g<sup>-1</sup>. Composite of PANI and GO sheets for the purpose of supercapacitor development is lately reported by Zhang *et al.* [30], which have synthesized *via* electrochemical method with high specific capacitance of 1136.4 F g<sup>-1</sup> with a GO concentration of 10 mg L<sup>-1</sup> at a scan rate of 1 mV s<sup>-1</sup>. Feng *et al.* [31] showed PANI-graphene composites synthesized by electrochemical reduction process with a high specific capacitance of 640 F g<sup>-1</sup>, and another composite synthesized by electropolymerization of PANI on the graphene electrode showing electrochemical capacitance of 223 F g<sup>-1</sup> [32]. PANI-graphene nanosheets composite with the specific capacitance of 1046 F g<sup>-1</sup> was synthesized using *in situ* polymerization [33].

In most of the work, the PANI is either be coated on graphene sheets or be covalently grafted on graphene sheets. However, very little attention has been paid to electrochemical co-deposition of PANI and GO together. This work describes the codeposition of PANI nanofibers and GO nanoplatelets in the form of thin films by using one-step electrochemical polymerization method. The as prepared PANI-GO films display remarkably enhanced electrochemical properties compare to the pure PANI thin film. The excellent electrochemical performance (supercapacitance, high power and high energy density) of PANI-GO films makes them promising electrode materials for electrochemical energy storage devices such as thin film microbatteries and ultracapacitors.

## 2. Experimental Section

### 2.1 Preparation of GO

GO was synthesized by a modified Hummers method [34-36]. Briefly, 2 g of graphite flakes (Nacional do Grafite; Graflake 99580; 99.50% purity) were dispersed in 98% (w/w) sulfuric acid at room temperature with a mechanical stirrer. After stirring for 15 min, 2 g of  $\text{KMnO}_4$  (Sigma-Aldrich) were slowly added to the suspension, which acquired a green color due to the formation of the oxidizing agent ( $\text{MnO}_3^+$ ). During this phase, the temperature was kept under  $30^\circ\text{C}$  by using an ice bath. Additional two portions of  $\text{KMnO}_4$  were added in a daily basis. The end of the oxidation was determined by the disappearance of the green color after adding the 3<sup>th</sup> portion of  $\text{KMnO}_4$ . At the end of the oxidation, the reaction mixture became very viscous due to the exfoliation of the formed GO layers. GO prepared by this described procedure was separated from the rest of the reaction mixture and purified. First, a few drops of 30% (w/w)  $\text{H}_2\text{O}_2$  were added until the purple color disappear. After this, the resulting mixture was centrifuged (Centribio, model 80-2B) at 1800 g until the supernatant became clear. The supernatant was removed and the precipitated was redispersed using an ice-water mixture, followed by other centrifugation at 1800 g. This cycle was repeated twice using water, other three times with 5% (v/v) HCl and finally washing twice with distilled water again. The time spent in the centrifugation until the supernatant became clear increased after each cycle. The resulted dispersion of GO in water ( $3.3 \text{ mg mL}^{-1}$ , pH  $\sim 5.0$ ) was stored at room conditions.

## 2.2 Electrodeposition of PANI-GO composite films

Aniline was obtained from Sigma-Aldrich, and distilled under vacuum to remove the oxidation impurities before use. Electrodeposition of PANI-GO and PANI films was carried out in a one-compartment three electrodes connected cell using a potentiostat (Autolab PGSTAT302N) electrochemical workstation at room temperature under computer control. The working and counter electrodes were indium-tin oxide (ITO) coated glass slides (Lumtec Corp.  $15 \Omega$ ) with a surface area of  $4 \text{ cm}^2$  and a platinum sheet with a surface area of  $4 \text{ cm}^2$ , respectively. ITO glass slides were carefully cleaned by a successive rinsing in the mixture of ethanol/acetone (1:1), and deionized water then dried under the gentle stream of nitrogen in sequence before use. The space between both electrodes was  $\sim 3 \text{ cm}$ , and saturated calomel electrode (SCE) was used as a reference electrode. In order to deposit PANI-GO on ITO substrate, an electrolyte solution of  $1 \text{ mol L}^{-1} \text{ H}_2\text{SO}_4 + 0.12 \text{ mol L}^{-1}$  aniline with varying the contents of GO suspension from 0.05 to 0.2 mL was prepared as follows: A controlled volume of aqueous colloidal suspension of GO ( $3.3 \text{ mg mL}^{-1}$ ) was added in 100 mL of  $1 \text{ mol L}^{-1} \text{ H}_2\text{SO}_4$  and ultrasonicated for 1 h (dispersion

was not very affected by ultrasonication), in the sequence, purified aniline monomer was added to this mixture and allowed to stir for 2 h at room temperature.

The electrolyte solutions were purged with nitrogen for 10 min before performing electrodeposition. For comparison, a pure PANI film was synthesized electrochemically in the absence of GO *via* similar procedure above. The all electrochemical deposition processes were carried out at a constant applied oxidative potential of 750 mV *vs.* SCE. The electrodeposited films were rinsed gently with double distilled water, dried under flowing nitrogen until a shiny green film has been obtained and stored in vacuum desiccators for several hours. Thus, the obtained PANI-GO films were labeled as PG-A, PG-B, and PG-C, for 0.05, 0.1, and 0.2 mL based on the feed amount of GO to the electrolyte solution, respectively. To investigate the mass of deposited material, a QCM200 Quartz Crystal Microbalance was used. The thickness of the films was measured by using Profilometer (Bruker). All solutions were prepared using Milli-Q grade water (18.2 M $\Omega$ .cm).

### 2.3 General characterization

The morphologies of the materials were investigated with a JEOL JSM-6701F field-emission scanning electron microscope (FE-SEM) and JEOL JSM-2100 transmission electron microscope (TEM). For FE-SEM analysis the electrodeposited film on ITO was mounted on aluminum stubs and sputter-coated with gold. For TEM analysis the small portion of the film was removed from ITO surface with the help of a spatula, sonicated in ethanol and then a drop of solution was dropped on copper microgrid. Infrared spectra (FTIR) were taken by of a Perkin-Elmer Tensor 100 spectrometer in the range of 400-4000 cm<sup>-1</sup>, pellets made from scratched material from ITO substrate and mixed with KBr. X-ray diffraction (XRD) patterns of the samples were recorded with Cu K $\alpha$  radiation at the scan rate of 2° (2 $\theta$ ) min<sup>-1</sup>. UV-visible (UV-vis) spectra of the samples were recorded from 200 to 1000 nm using a Perkin Elmer 750 spectrophotometer. XPS (X-ray photoelectron spectroscopy) were collected using a Phi Quantum 2000 (Physical Electronics) instrument with monochromatized Al K $\alpha$  as the radiation source.

### 2.4 Current sensing AFM characterization

Current sensing atomic force microscopy (CS-AFM) measurements were performed in air using a Pico-SPM (Molecular Imaging Corporation, USA) AFM operating in contact mode. Pt/Ir

coating tips with the nominal force constant of 0.2 N/m and tip curvature radius of 20 nm were used for simultaneously imaging of topography and mapping of the local changes of electric conductance of the sample surface. Samples for CS-AFM studies were mounted via silver paste, to the AFM sample holder. I/V curves using the CS-AFM system on different points on the film surface were also performed to obtain the local character of electric conductance. The I/V curves are the average of at least 20 measurements and the image treatment and analysis were carried out using WSxM 4.0 Develop 12.1 software.

### 2.5 Electrochemical characterization

To evaluate the electrochemical experiments, the device was connected to an electrochemical workstation using alligator clips. The electrochemical behavior of the PANI-GO films was evaluated using cyclic voltammetry (CV), galvanostatic charge-discharge measurements, and electrical impedance spectroscopy (EIS). All electrochemical experiments were carried out in 1 mol L<sup>-1</sup> H<sub>2</sub>SO<sub>4</sub>. The EIS analysis of the sample was done by superimposing a sinusoid perturbation of 5 mV over a zero applied voltage and measuring the in-phase and out-phases current components for frequencies ranging from 10 mHz to 100 kHz. Two consecutive experiments were done for each sample, where the first experiment was discarded to avoid charging effects. The equipment employed was a FRA 2 model in an Autolab potentiostat. All electrochemical tests were carried out in a three electrode cell, where the counter electrode was a platinum foil, working electrode was an electrodeposited film, and a SCE was used as reference electrode.

### 3. Results and Discussion

The current vs. time (I/t) curves were recorded during the electrochemical deposition of PANI-GO films and pure PANI film at a constant applied oxidative potential of 750 mV, as shown in Fig. 1. All I/t curves follow the same trend with current increasing gradually until reaching a saturation level [37]. In the electrolyte, the presence of protonic acid H<sub>2</sub>SO<sub>4</sub> that provides necessary counter ions where the imine nitrogens of PANI are protonated. A wide range of oxygen functionalities (-OH, C-O-C, -COOH) bonded onto the surface of GO electrostatically interact with aniline monomer and makes the complex in aqueous electrolyte solution. As the electropolymerization of aniline is done the deposited PANI films contain both acid counter ion

and GO onto electrode surface. The incorporation of acid counter ion in the PANI-GO film was verified by XPS analysis.

It is also expected that the oxygen functionalities of GO as the charge compensating sites which interact with the radical cations of the NH groups of the emeraldine salt form of PANI. The electrochemical properties of the PANI-GO films were compared with pure PANI film having acid counter ion only. The electrochemical setup and the digital images of electrodeposited films as well as the possible interactions between aniline-GO and PANI-GO are illustrated in Fig. 2. The all samples that were further investigated in this work had thin solid films with thickness of about  $148 \pm 5$  nm. The weight of deposit material has been recorded using a QCM. By taking into account the electrodeposited charge as a function of time and the thickness of the layers at different deposition times, it was possible to calculate the mass density for PANI sample with and without GO using the Equation below:

$$\rho = \frac{M\alpha}{QA} \quad \text{Eq. 1}$$

where  $\rho$  is the mass density, M is the electroplated mass, Q is the electrodeposited charge, A is the delimited area, and  $\alpha$  is proportionality constant between charge and thickness in C/cm. Fig. 3. displays the calculated mass density of each film for the different amounts of GO in electrolyte. All samples present the same behavior, a rapid increase of density in the initial stages of electrodeposition, this effect can be attributed to a high compact grow of PANI nanofibers. Nevertheless, after a dozens of nanometers thicknesses, the mass density start to fall slowly, indicating the nucleation of fibers and other non-compact structures. Visible differences between PANI-GO deposit samples can be seen, *i.e.*, by raising the amount of GO in the electrolyte, films become heavier. The linear relation between thin film mass and GO amount in the electrolyte is shown in the inset of figure indicating that the mass of the films increased with increasing the amount of GO in the electrolyte. The mass of deposit materials were 60, 68, 82, and 120  $\mu\text{g}$  for pure PANI, PG-A, PG-B, and PG-C samples, respectively.

### 3.1 Morphological and structural characterization

The typical micromorphology of the resulting films was observed by FE-SEM and TEM. The FE-SEM micrographs of pure PANI and PANI-GO films as presented in Fig. 4, shows the

microstructure of PANI nanofibers with and without GO. Random and highly interconnected network fibrillar morphology was observed for all samples. It could be seen that for all PANI-GO samples the PANI nanofibers accompanied with GO platelets as large as 1  $\mu\text{m}$  size. TEM imaging was used to determine the detailed nanoscale structure of PANI-GO films, as can be seen in Fig. 5. A close examination of individual nanofibers morphology indicates the stacking of GO platelets onto the surface of PANI nanofibers (Fig. 5 c-d) as compared to the pure PANI nanofibers (Fig. 5 a-b). The GO platelets with PANI nanofibers are suggesting a good compatibility between both components. PANI is a conducting polymer that contains positively charged nitrogen on its polymer chain which favors the adhesion of GO platelets onto the PANI nanofibers. Hence, it is no wonder that the unique structure of PANI-GO can be considered for high electrochemical performance.

Fig. 6 shows results obtained with AFM and current sensing measurements. The CS-AFM is a powerful technique for characterization the conductivity of the sample surface. The microscope can apply a constant voltage and monitor the current between the sample and the probing tip during the scan. The 3D representation (Fig. 6 a) of the topography of bare ITO, pure PANI and PANI-GO samples reveals the rough nature of electrodeposited surfaces. For bare ITO and pure PANI a roughness (root mean square fluctuation of height) below 3 nm was measured. The roughness increased significantly with the increase of GO contents in the films, 26 nm for PG-A and 48 nm for PG-C. The rougher surface of PANI-GO films provides a high accessible surface area for the redox activity. The whole surface area of the electrodeposited films was conductive at an applied bias of 4 V. In Fig. 6 b, the I/V curve for bare ITO shows the ohmic behavior while the I/V curves for pure PANI and PANI-GO films show the typical semiconductor behavior. The differences in shape of these I/V curve due to the inhomogeneous surface of the films. The current passing through different nanofibers is not same due to the non-uniformity in height of the nanofibers, as we also can see in SEM results.

The XPS spectrum of the electrodeposited PANI-GO film was obtained to verify the presence of GO and PANI. The XPS spectra of PANI-GO and GO were analyzed, and the comparative results are shown in Fig. 7. The spectrum of PANI-GO (Fig. 7 a) in regard of spectrum of GO (Fig. 7 b), shows two new peaks correspond to the N 1s and S 2p, the peak N 1s comes from PANI and the peak S 2p comes from sulfuric acid, respectively. The presence of S 2p peak in the PANI-GO film indicates that the PANI was also doped by sulfuric acid. As a

result, this is a clear signal of coexistence of both PANI and GO in the electrodeposited film. The core level spectrum of C 1s for PANI-GO film is shown in supporting information (Fig. SI 4), where the curves fit for various carbon components i.e., C-C, C-O, C=O, and C-N due to the presence of oxygen and nitrogen species. Signals for C-O and C=O, it is the evidence of GO and the signal for C-N, it is the evidence of PANI. Further evidence in the coexistence of the GO and PANI in the electrodeposited films was provided by the FT-IR spectra as shown in Fig. 8. A typical FT-IR spectrum of GO is shown in Fig. 8 a. In agreement with previous work [38,39], the spectrum shows several bands broad band centered at  $3430\text{ cm}^{-1}$  is attributed to deformation of -OH group, the band at  $1740\text{ cm}^{-1}$  is due to carbonyl or carboxylic groups (C=O), the band around  $1635\text{ cm}^{-1}$  is due to aromatic C=C, and the band at  $1460\text{ cm}^{-1}$  is due to carboxy (C-O), epoxy C-O ( $1260\text{ cm}^{-1}$ ), and alkoxy C-O ( $1105\text{ cm}^{-1}$ ) groups located at the edges and basal planes of GO. The FT-IR spectrum of the electrochemically prepared pure PANI in Fig. 8 b shows the bands at  $1645\text{ cm}^{-1}$  and  $1560\text{ cm}^{-1}$  of the quinonoid and benzenoid units, respectively [40-42]. The bands at  $1295$  and  $1260\text{ cm}^{-1}$  are assigned to the C-N stretching of benzenoid unit while the band at  $1095\text{ cm}^{-1}$  is due to C=N stretching of quinonoid which are identical to that of doped PANI, and many low-intensity peaks ranging from  $800$  to  $500\text{ cm}^{-1}$  can be assigned to the vibrations of the C-H bonds in the benzene rings [43,44]. The broad peak in the frequency range of  $3445\text{ cm}^{-1}$  is attributed to the N-H stretching vibrations of the emeraldine salt and the shoulders at  $2850$ - $2995\text{ cm}^{-1}$  correspond to aromatic  $\text{sp}^2$  C-H stretching [45]. The spectrum (Fig. 8 c) of PANI-GO film is showing all characteristics peaks of both PANI and GO. It also noticed that the low intensity peak at  $1299\text{ cm}^{-1}$  in the spectrum of pure PANI becomes more intense in the spectrum of PANI-GO, which is caused by the strong interaction between the amine group of PANI and oxygenated GO, which clearly supports the adsorption of GO nanoplatelets with PANI nanofibers during electropolymerization process.

UV-vis spectra of electrodeposited PANI-GO film on ITO display basically the same absorptive characteristics as that of electrodeposited pure PANI film ( $\text{H}_2\text{SO}_4$  doped) as shown in Fig. 9 b & c). The peaks at  $\sim 300$  and  $800\text{ nm}$  are attributed to benzenoid rings and quinoid rings, respectively [46, 47]. Additionally, after adsorption of GO nanoplatelets onto PANI nanofibers, the peak at  $284\text{ nm}$  of the PANI-GO film blue shifts by  $15\text{ nm}$  compared to the pure PANI film, indicating the interaction of GO with PANI. The absorption peak of the GO could be observed at  $215\text{ nm}$  (Fig. 9 a). The structure of the PANI-GO film was also examined by powder XRD

measurements. The XRD patterns of pure PANI and PANI-GO samples (PG-B, and PG-C) are shown in Fig. 10. The pure PANI exhibits several broad reflection peaks with the most intense peaks centered at  $2\theta = 25^\circ$ , and the peak at  $2\theta = 5.9^\circ$  can be ascribed to the orientation of the acids ( $\text{H}_2\text{SO}_4$ ) in the polyaniline chain [40-50]. Upon anchor of GO nanoplatelets onto PANI nanofibers, the peaks have widened in comparison with the pattern of pure PANI nanofibers which has been believed to the reflection of GO nanoplatelets. Therefore, XRD result verifies the presence of GO into the electrodeposited PANI-GO film.

### 3.2 Electrochemical performance of PANI-GO thin film electrodes

All electrochemical measurements were based on three electrode cell system. A platinum sheet was used as counter electrode, SCE electrode was used as a reference electrode and the thin films of PANI-GO and pure PANI on ITO substrate was used as working electrodes. The electrolyte ( $1 \text{ mol L}^{-1} \text{ H}_2\text{SO}_4$ ) was used for all electrochemical tests. Fig. 11 a) illustrates the CV curves of samples PG-A, PG-B, PG-C, and pure PANI at the scan rate of  $10 \text{ mV/sec}$  in the potential window of  $-0.2$  to  $0.8 \text{ V}$ . From the figure, the remarkable difference of electrochemical surface activity between pure PANI and PANI-GO films can be easily recognized. The redox current peak of pure PANI film is much lower compared to PANI-GO films at the same scan rate of  $10 \text{ mV/sec}$ . It is commonly believed that the electrochemical capacitance is proportional to the area under the CV curve; the area under CV curves of PANI-GO films is much larger than pure PANI film. This sign is indicating a typical pseudocapacitance behavior of PANI-GO films, caused by redox reaction at the electrode. The PANI undergoes intrinsic redox process electrochemically. The CV curves of PANI-GO films demonstrate the three couples of redox peaks (aa', bb' and cc') in the range of  $-0.1$  to  $+0.7 \text{ V}$ , where the redox pair aa' correspond to the reversible transition between leucoemeraldine form (reduced form of PANI) and emeraldine form of PANI (half-oxidized form of PANI) [51]. The redox pair cc' is ascribed to reversible transition between emeraldine and pernigraniline (fully oxidized form of PANI) [52]. The middle pair bb' either is transition between benzoquinone/aminoquinone couple of PANI [53] or may be due to the transition between quinone/hydroquinone groups of GO [54].

This observation indicates that the total capacitance of PANI-GO film could be mainly dominated by the Faradaic reactions at the electrode/electrolyte surface, which is different from the electric double layer capacitance of carbon-based materials. Here, it can be speculated that

the introduction of GO induce the synergistic effect between PANI nanofibers and GO nanoplatelets as well as improving the electrode/electrolyte contact surface area for electronic or electrolyte ion transport, which is valuable for enhancing the use of active materials [29, 51]. Such electrochemical properties indicate that in this investigation PG-C is the most promising material for use in supercapacitor thin film electrode of this type. To further investigate the influence of the scan rates we measured the rate dependant cyclic voltammograms of PANI-GO (PG-C) electrode at the range from 10 to 25 mV/sec. It can be found from Fig. 11 b that the PANI-GO film exhibit similar curves as the scan rate increase from 10 to 25 mV/sec, indicating a good rate capability of PANI-GO electrode film. It is also important to note that the cathodic peak shift positively with increasing the sweep rates from 10 to 25 mV/sec. The positive shifting of cathodic peak is mainly due to a slight increase in the resistance of the electrolyte at high sweep rates. We also observed the electrochromic behavior of the films during CV experiment; PANI-GO films were showing the change in color (dark green to light green and vice versa, as shown by schematic diagram in Fig 11 b).

The specific capacitance values were assessed by galvanostatic charge-discharge cycling measurements. This method is more reliable to characterize the capacitance of the materials under controlled current conditions. The capacitance values of the samples were estimated according to the following equation: specific capacitance ( $F/g$ ) =  $I / (m dV/dt)$ . Here,  $I$  is the discharge current in amperes,  $m$  is the mass (gram) of active material on the substrate, and  $dt$  is the discharge time (sec) corresponding to the voltage difference  $dV$  in volts.  $dV/dt$  can be obtained from the slop of the discharge curve. The galvanostatic charge-discharge cycles were examined at various current densities from 0.025 to 0.25 mA cm<sup>-2</sup>. The curve of PANI-GO films in Fig. 12 a show longer charge-discharge duration than pure PANI film, which means that it possesses higher specific capacitance than pure PANI. A high specific capacitance value of 662 F g<sup>-1</sup> was obtained for sample PG-C at a constant low current density of 0.025 mA cm<sup>-2</sup>, whereas the pure PANI film has minimal capacitance of 256 F g<sup>-1</sup> at the same current density. Thus, the greatly increased specific capacitance can be ascribed from the synergistic contribution of PANI nanofibers and GO nanoplatelets together with the merits of interconnected nanofibers porous structure of the film. In other words, individually both components cannot offer high specific capacitance but together provides enhanced electrode/electrolyte interface area accessible for redox reaction during charge-discharge processes, and made them fully electrochemically

accessible. Therefore, the electrochemical property of the PANI-GO was improved effectively. The variation of the specific capacitance with the current density is shown in Fig. 12 b. It shows that the specific capacitance decreases significantly with the increment of scan current density, and can be achieved as high as  $580 \text{ F g}^{-1}$  even at a ten times higher discharge current density of  $0.25 \text{ mA cm}^{-2}$ . This marks the good rate capability of the PANI-GO film (PG-C), which is recognized as one of the most important electrochemical properties in the application of thin film electrode materials.

Thus, we believe that in our system the high capacitance of electrodeposited PANI-GO films is anticipated due to the unique microstructure of materials which provide the ideal synergistic interaction between PANI nanofibers and GO nanoplatelets. The electrochemical stability of PG-C film was examined under continuous charge discharge tests at  $0.1 \text{ mA cm}^{-2}$  for 100 cycles. As shown in Fig. 13, there is a small decrease in the specific capacitance value of sample PG-C in the 100 cycles and thereafter, the specific capacitance remains almost constant. The decrease in the specific capacitance was 10% in the 100 cycles. The instability of the capacitors based on electrochemically prepared films during long-term charge-discharge cycling experiment is one of the most serious problem. Our films could not be reused after prolonged experiment because the electrodeposited film of PANI-GO was started to peel off from the ITO surface. To overcome this drawback, the work is undergoing in our lab for making more long-lasting thin film electrode having high specific capacitance. Energy density and power density are also used as important factors for supercapacitors. Specific energy and specific power have been derived from galvanostatic charge-discharge at various current densities using the following equations: specific energy ( $\text{Wh kg}^{-1}$ ) =  $[I \times t \times V]/m$ , and specific power ( $\text{W kg}^{-1}$ ) =  $[I \times V]/m$ , where discharge current ( $I$ ), time ( $t$ ) spent in discharge, mass ( $m$ ), and voltage ( $V$ ) are in amperes, seconds, kilogram, and volts, respectively. The evaluated values of specific energy and specific power are shown in Fig. 14. At the specific energy of  $64.5 \text{ Wh kg}^{-1}$ , a specific power of  $1159 \text{ W kg}^{-1}$  was obtained at the current scan rate of  $1.6 \text{ A g}^{-1}$ . The specific power as high as  $17500 \text{ W kg}^{-1}$  was obtained with the specific energy of  $34 \text{ Wh kg}^{-1}$  at the current scan rate of  $25 \text{ A g}^{-1}$ . These values are comparable with the earlier reported results for thin film electrode materials in the three electrodes cell system [55, 56].

Electrical characterization was performed for all samples in  $1 \text{ mol L}^{-1} \text{ H}_2\text{SO}_4$  aqueous electrolyte by the electrochemical impedance spectroscopy (EIS). This is a useful technique to

analyze the frequency dependent electrochemical response of the system. The EIS data have been analyzed by using Nyquist plots. This plot shows the frequency response of the electrode/electrolyte system and is a plot of the imaginary component ( $\text{Im}\{Z\}$ ) of the impedance against the real component ( $\text{Re}\{Z\}$ ). Fig. 15 displays Nyquist plot for PANI and PANI-GO samples, the semicircle for high frequency region and the vertical linear characteristic in the mid-to-low frequency regions were observed. The circuit parameters such as series impedance, charge transport impedance, and characteristic frequencies were extracted by fitting the semicircles assuming that the system response follows a modified Randle circuit. We observed that the double layer charge transport has a characteristic frequency of 2.4 kHz for pure PANI film and 370 Hz for PANI-GO films. The electrical resistivities calculated by using charge transport resistance values at 0 V were 1.5 M $\Omega$ .cm for pure PANI and between 5 to 9 M $\Omega$ .cm for PANI-GO samples. The electrolyte resistance was only observed for PANI samples of about 16  $\Omega$ , due to frequency limitations. The resistance is increasing with increasing amount of GO in the electrolyte mixture due to nonconductive nature of GO. Here, it is in contrast with Zhang reported work [57], he found, when composited with PANI, GO demonstrates higher conductivity at lower concentration due to the increase of the doping degree of PANI. Since the charge transport resistance remains almost constant, the lower frequencies observed for PANI-GO samples could be attributed to an increase in the capacitance of the samples.

#### 4. Conclusions

In conclusion, composite thin films of graphene oxide nanoplatelets and polyaniline nanofibers have been successfully codeposited by using simple one-step electrochemical method. The resulting films have a dense interconnected nanofibers structure and appear to consist GO nanoplatelets in SEM and TEM images. Thus obtained PANI-GO films exhibited excellent electrochemical properties. The greatly enhanced electrochemical performances of PANI-GO thin film electrodes are due to synergistic combination between the PANI nanofibers and GO nanoplatelets. The specific energy of the thin film electrode material is evaluated at several specific power values and Ragone diagram is plotted. Further optimization may be possible by fine-tuning of the synthetic conditions. The approach described here may be applicable to other conducting polymers with GO nanoplatelets. Such thin film electrode materials are inevitably required for thin film microbatteries and ultracapacitors.

## Acknowledgements

Author M.K. would like to place in record his special thanks to the CAPES/PNPD, Government of Brazil for providing postdoctoral fellowship to carry out part of the research work in the physics department of UFSC, Florianopolis. The authors also thank to Prof. A. Neves (LBC/UFSC, Brazil) for providing FTIR facility and other Brazilian funding agencies FINEP, CNPq and FAPESC.

## References:

- 1 P. Simon, Y. Gogotsi, *Nat. Mater.*, 2008, **7**, 845-854.
- 2 M. Jayalakshmi, K. Balasubramanyam, *Int. J. Electrochem. Sci.*, 2008, **3**, 1196-1217.
- 3 C. Yuan, B. Gao, L. Shen, S. Yang, L. Hao, J. X. Lu, F. Zhang, J. L. Zhang, G.X. Zhang, *Nanoscale*, 2011, **3**, 529-545.
- 4 S. W. Lee, B. M. Gallant, H. R. Byon, P. T. Hammond, Y. Shao-Horn, *Energy Environ Sci.*, 2011, **4**, 1972-1985.
- 5 M. Liu, Y. E. Miao, C. Zhang, W. W. Tjiu, Z. Yang, H. Peng, T. Liu, *Nanoscale*, 2013, **5**, 7312-7320.
- 6 K. R. Prasad, N. Munichandraiah, *J. Pow. Sour.*, 2002, **112**, 443-451.
- 7 M. Mecklenburg, A. Schuchardt, Y. K. Mishra, S. Kaps, R. Adelung, A. Lotnyk, L. Kienle, K. Schulte, *Adv. Mater.*, 2012, **24**, 3486-3490.
- 8 X. B. Yan, Z. X. Tai, J. T. Chen, Q. J. Xue, *Nanoscale*, 2011, **3**, 212-316.
- 9 S. X. Xiong, F. Yang, H. Jiang, J. Ma, X. H. Lu, *Electrochim. Acta*, 2012, **85**, 235-242.
- 10 X. J. Lu, H. Dou, S. D. Yang, L. Hao, L. J. Zhang, L. F. Shen, F. Zhang, X. G. Zhang, *Electrochim. Acta*, 2011, **56**, 9224-9232.
- 11 F. Kim, L. J. Cote, J. Huang, *Adv. Mater.*, 2010, **22**, 1954-1958.
- 12 H. He, J. Klinowski, M. Forster, A. Lerf, *Chem. Phys. Let.*, 1998, **287**, 53-56.
- 13 A. Lerf, H. He, M. Forster, J. Klinowski, *J. Phy. Chem. B*, 1998, **102**, 4477-4482.
- 14 G. Wang, W. Xing, S. Zhuo, *Electrochim. Acta*, 2012, **66**, 151-157.
- 15 K. Zhang, L. L. Zhang, X. S. Zhao, J. Wu, *Chem. Mater.*, 2010, **22**, 1392-1401.
- 16 E. Coskun, E. A. Z-Contreras, H. J. Salavagione, *Carbon*, 2012, **50**, 2235-2243.
- 17 Z. Cui, C. X. Guo, W. Yuan, C. M. Li, *Phys. Chem. Chem. Phys.*, 2012, **14**, 12823-12828.

- 18 A. K. Mishra, S. Ramaprabhu, *J. Mater. Chem.*, 2012, **22**, 3708-3712.
- 19 H. L. Wang, Q. L. Hao, X. J. Yang, L. D. Lu, X. Wang, *ACS Appl. Mater. Inter.*, 2010, **2**, 821-828.
- 20 B. Xu, S. F. Yue, Z. Y. Sui, X. T. Zhang, S. S. Hou, G. P. Cao, Y. S. Yang, *Ener. Envir. Sci.*, 2011, **4**, 2826-2830.
- 21 S. Liu, X. H. Liu, Z. P. Li, S. R. Yang, J. Q. Wang, *New J. Chem.*, 2011, **35**, 369-374.
- 22 Q. Wu, Y. X. Xu, Z. Y. Yao, A. R. Liu, G. Q. Shi, *ACS Nano*, 2010, **4**, 1963-1970.
- 23 Y. Li, H. Peng, G. Li, K. Chen, *Eur. Polym. J.*, 2012, **48**, 1406-1412.
- 24 J. Li, H. Xie, Y. Li, J. Liu, Z. Li, *J. Pow. Sour.*, 2011, **196**, 10775-10781.
- 25 H. Gomez, M. K. Ram, F. Alvi, P. Villalba, E. Stefanakos, A. Kumar, *J. Pow. Sour.*, 2011, **196**, 4102-4108.
- 26 F. Chen, P. Liu, Q. Zhao, *Electrochim. Acta*, 2012, **76**, 62-68.
- 27 G. Wang, S. Zhuo, W. Xing, *Mater. Lett.*, 2012, **69**, 27-29.
- 28 W. L. Zhang, Y. D. Liu, H. J. Choi, *Carbon*, 2012, **50**, 290-296.
- 29 J. J. Xu, K. Wang, S. Z. Zu, B. H. Han, Z. X. Wei, *ACS Nano*, 2010, **4**, 5019-5026.
- 30 Q. Zhang, Y. Li, Y. Feng, W. Feng, *Electrochim. Acta*, 2013, **90**, 95-100.
- 31 X. M. Feng, R. M. Li, Y. W. Ma, R. F. Chen, N. E. Shi, Q. L. Fan, W. Huang, *Adv. Func. Mat.*, 2011, **21**, 2989-2996.
- 32 D. W. Wang, F. Li, J. P. Zhao, W. C. Ren, Z. G. Chen, J. Tan, Z. S. Wu, L. Gentle, G. Q. Lu, H. M. Cheng, *ACS Nano*, 2009, **3**, 1745-1752.
- 33 J. Yan, T. Wei, B. Shao, Z. J. Fan, W. Z. Qian, M. L. Zhang, F. Wei, *Carbon*, 2010, **48**, 487-493.
- 34 A. Dimiev, D. V. Kosynkin, L. B. Alemany, P. Chaguine, J. M. Tour, *J. Am. Chem. Soc.*, 2012, **134**, 2815-2822.
- 35 W. S. Hummers, R. E. Offeman, *J. Am. Chem. Soc.*, 1958, **80**, 1339-1339.
- 36 L. J. Cote, F. Kim, J. Huang, *J. Am. Chem. Soc.*, 2009, **131**, 1043-1049.
- 37 H. Randriamahazaka, V. Noel, C. Chevrot, *J. Electroanal. Chem.*, 1999, **472**, 103-111.
- 38 X. Huang, N. Hu, R. Gao, Y. Yu, Y. Wang, Z. Yang, E. S-W. Kong, H. Weia, Y. Zhang *J. Mater. Chem.*, 2012, **22**, 22488-22495.
- 39 Y. Zhao, G-S. Tang, Z-Z. Yu, J-S. Qi, *Carbon*, 2012, **50**, 3064-3073.
- 40 Z. Ping, H. Neugebauer, A. Neckel, *Electrochim. Acta*, 1996, **41**, 767-772.

- 41 Z. Ping, G. E. Nauer, H. Neugebauer, J. Theiner, A. Neckel, *J. Chem. Soc. Faraday Trans.*, 1997, **93**, 121-129.
- 42 A. Kellenberger, E. Dmitrieva, L. Dunsch *J. Phys. Chem., B*, 2012, **116**, 4377-4385.
- 43 Y. Li, X. Zhao, Q. Xu, Q. Zhang, D. Chen, *Langmuir*, 2011, **27**, 6458-6463.
- 44 H. Gu, Y. Huang, X. Zhang, Q. Wang, J. Zhu, L. Shao, N. Haldolaarachchige, D. P. Young, S. Wei, Z. Guo, *Polymer*, 2011, **53**, 801-809.
- 45 X. B. Yan, Z. J. Han, Y. Yang, B. K. Tay, *Sens. Actu. B*, 2007, **123**, 107-113.
- 46 J. X. Huang, S. Virji, B. H. Weiller, R. B. Kaner, *J. Am. Chem. Soc.*, 2003, **125**, 314-315.
- 47 J. X. Huang, R. B. Kaner, *J. Am. Chem. Soc.* 2004, **126**, 851-855.
- 48 Z. M. Zhang, M. X. Wan, Y. Wei, *Adv. Funct. Mater.* 2006, **16**, 1100-1104.
- 49 T. Jana, J. Chatterjee, A. K. Nandi, *Langmuir*, 2002, **18**, 5720-5727.
- 50 Z. D. Zujovic, C. Laslau, G. A. Bowmaker, P. A. Kilmartin, A. L. Webber, S. P. Brown, J. Trivas-Sejdic, *Macromolecules*, 2010, **43**, 662-670.
- 51 Y. G. Wang, H. Q. Li, Y. Y. Xia, *Adv. Mater.*, 2006, **18**, 2619-2623.
- 52 C. C. Hu, C. H. Chu, *Mater. Chem. Phys.*, 2000, **65**, 329-238.
- 53 Y. H. Lee, C. Z. Chang, S. L. Yau, L. J. Fan, Y. W. Yang, *J. Am. Chem. Soc.*, 2009, **131**, 6468-6474.
- 54 Y. R. Nian, H. S. Teng, *J. Electrochem. Soc.*, 2002, **149**, A 1008-1014.
- 55 Md. M. Sk, C. Y. Yue, R. K. Jena, *Polymer*, 2014, **55**, 798-805.
- 56 V. Gupta, N. Miura, *Electrochem. Sol. Sta. Lett.*, 2005, **8**, A630-A632.
- 57 K. Zhang, L. L. Zhang, X. S. Zhao, J. S. Wu, *Chem. Mat.*, 2010, **22**, 1392-1401.

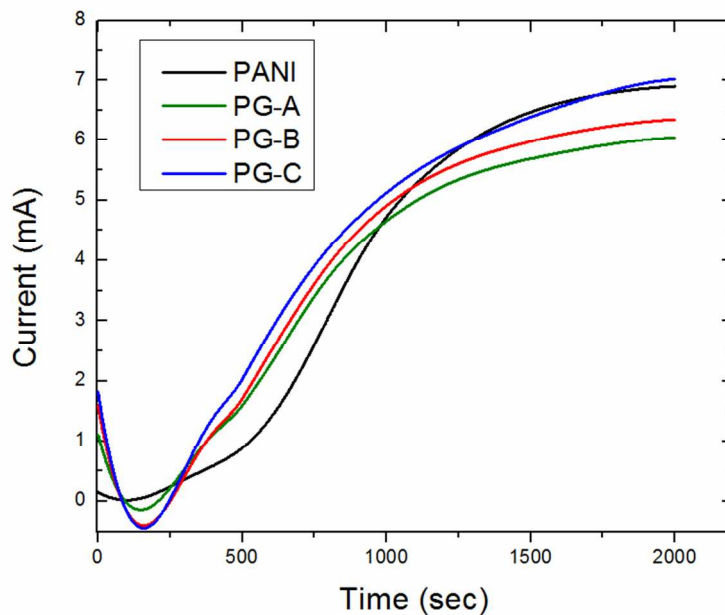


**Fig. 1** Current vs. time transients recorded during electrodeposition at a constant oxidative potential of 750 mV. The electrolyte mixture was 0.12 mol L<sup>-1</sup> aniline in 100 mL aqueous solutions of 1 mol L<sup>-1</sup> H<sub>2</sub>SO<sub>4</sub> + 0.05, 0.1, and 0.2 mL of GO colloidal suspension in a question of PG-A, PG-B, and PG-C samples, respectively.

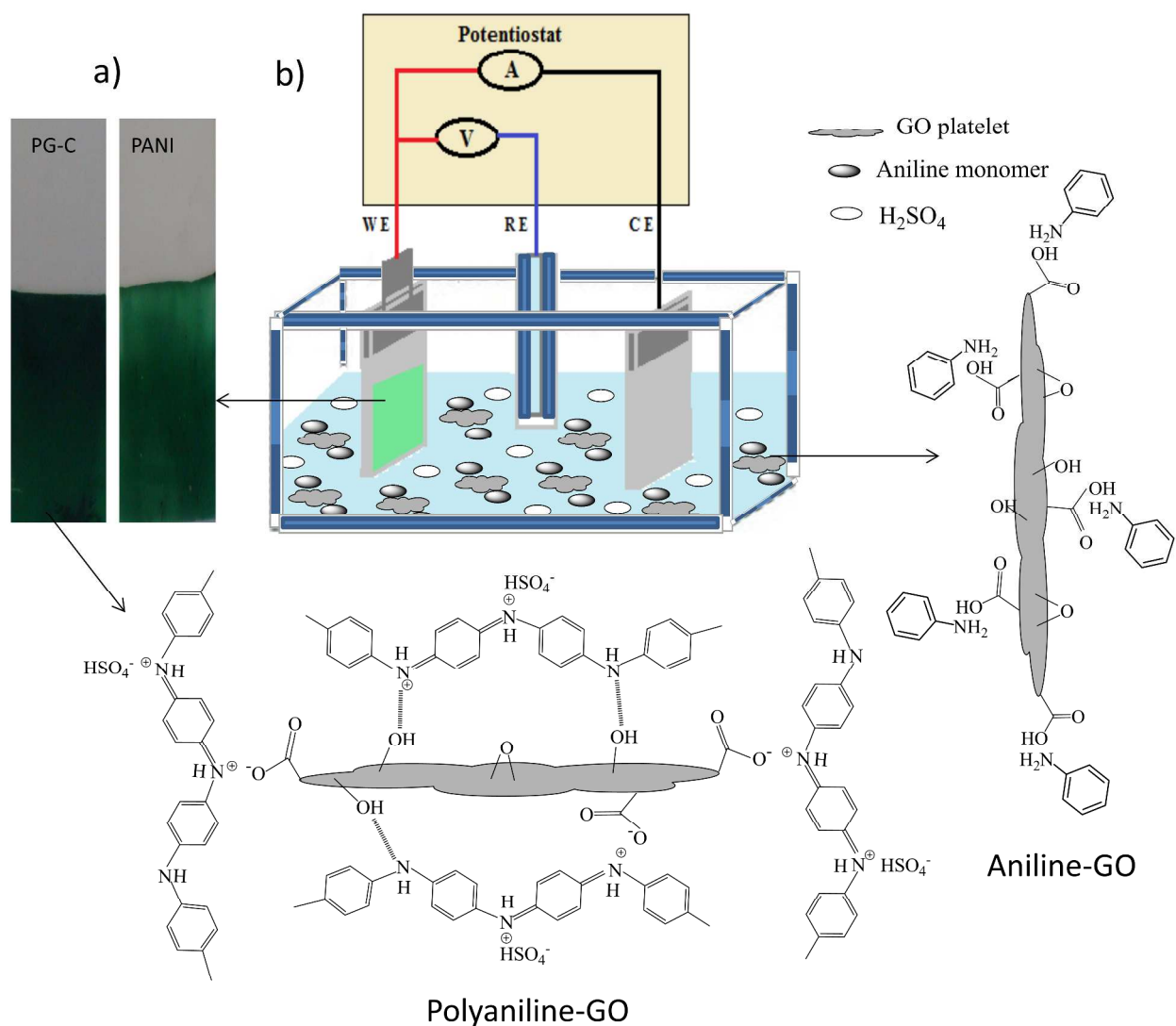


**Fig. 2** a) Representative digital photographs of pure PANI and PANI-GO thin films on ITO-coated glass slides, and b) Experimental setup of electrochemical deposition and illustration of multiple possible interactions between aniline-GO and PANI-GO.

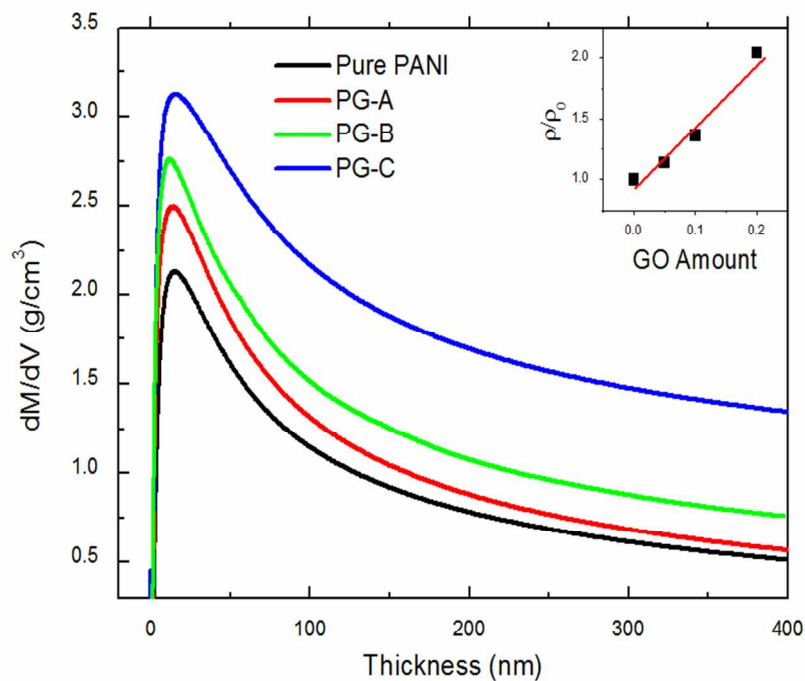


**Fig. 3** Calculated mass density vs. thickness and inset shows the relative mass density vs. GO amounts, where  $\rho_0$  = mass density of pure PANI and the curve obtained at 150 nm thickness of the films.

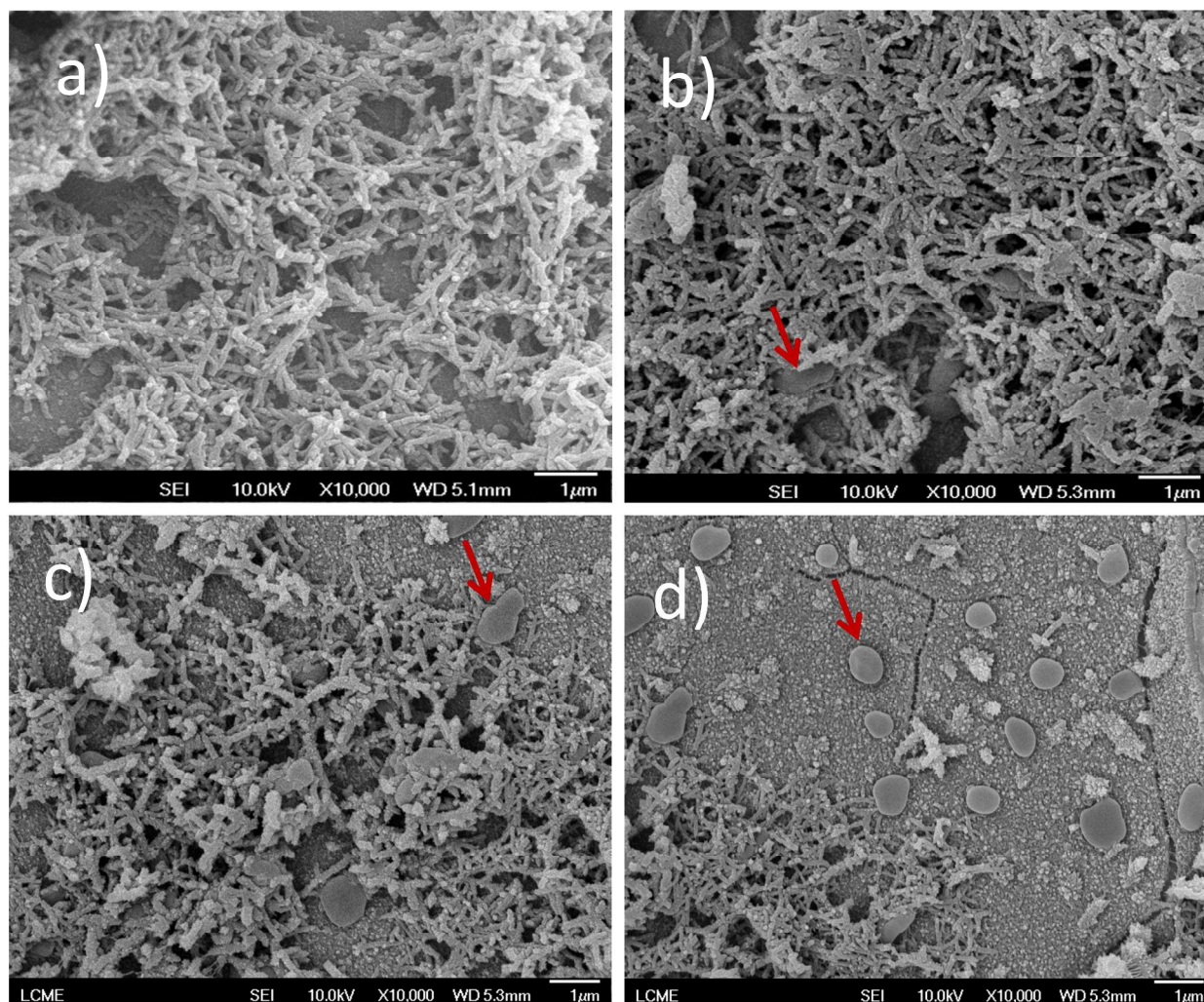


**Fig. 4** SEM images of interconnected network of nanofibers of (a) pure PANI, and (b-d) PAN-GO samples (PG-A, PG-B and PG-C), where the red arrow point to the some big size platelets of GO embedded with PANI nanofibers.

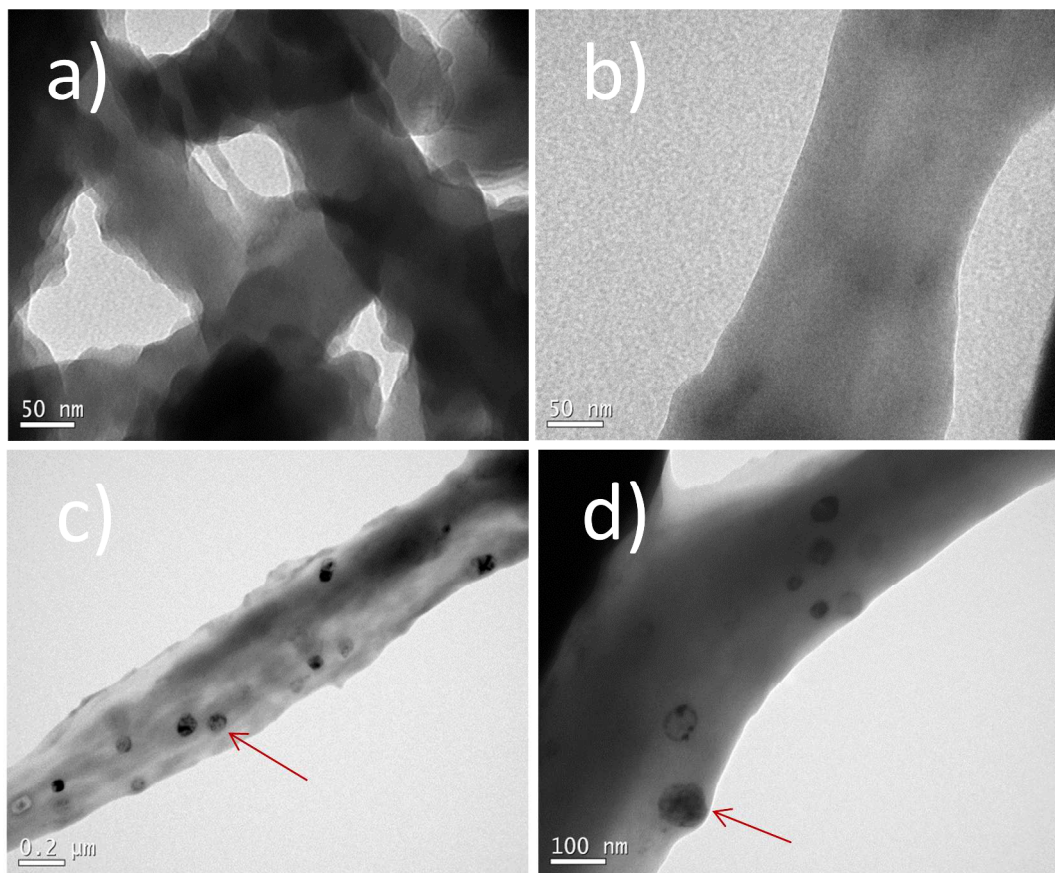


**Fig. 5** (a-b) TEM images of pure PANI nanofibers/nanofiber, and (c-d) TEM images of PANI-GO samples PG-C at different magnification. The red arrows point to the stacking of GO nanoplatelets onto the PANI nanofibers.

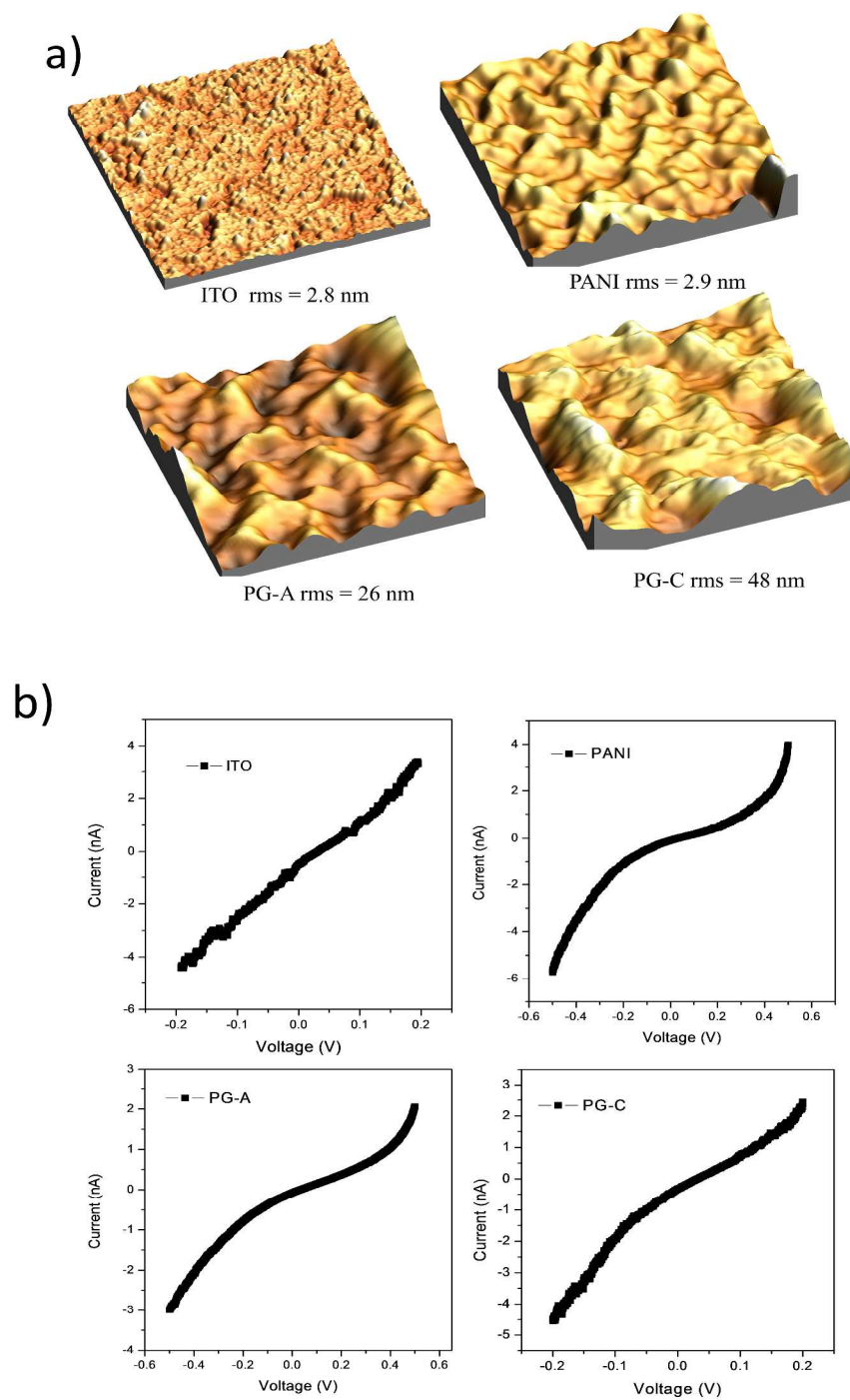


**Fig. 6** Topographical 3D AFM images of a) bare ITO, pure PANI, PG-A, and PG-C, (rms = root mean square of the surface roughness of the films), b) I/V curves of bare ITO, pure PANI, and PANI-GO samples (PG-A, and PG-C).

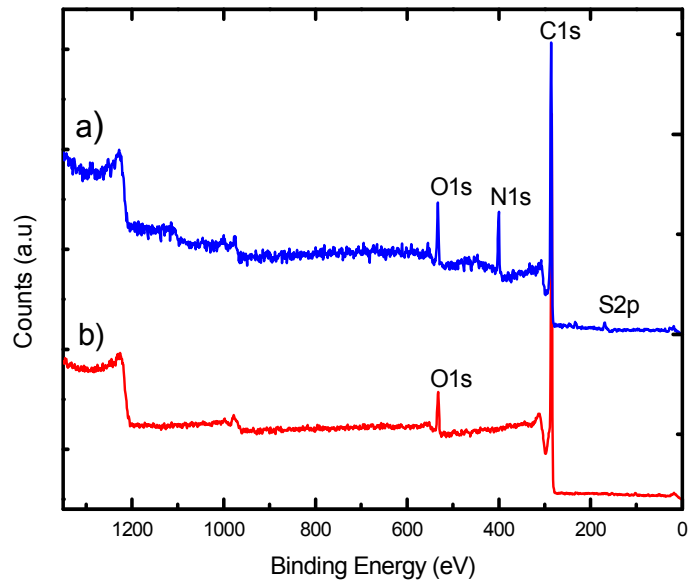


**Fig. 7** a) XPS spectrum of PANI-GO film (PG-C), and b) XPS spectrum of GO.

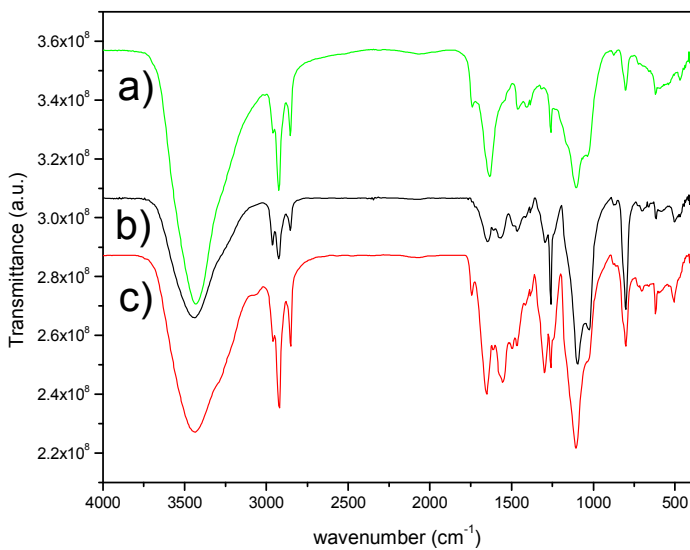


**Fig. 8** FTIR spectra of a) GO, b) pure PANI, and c) PANI-GO (PG-C).

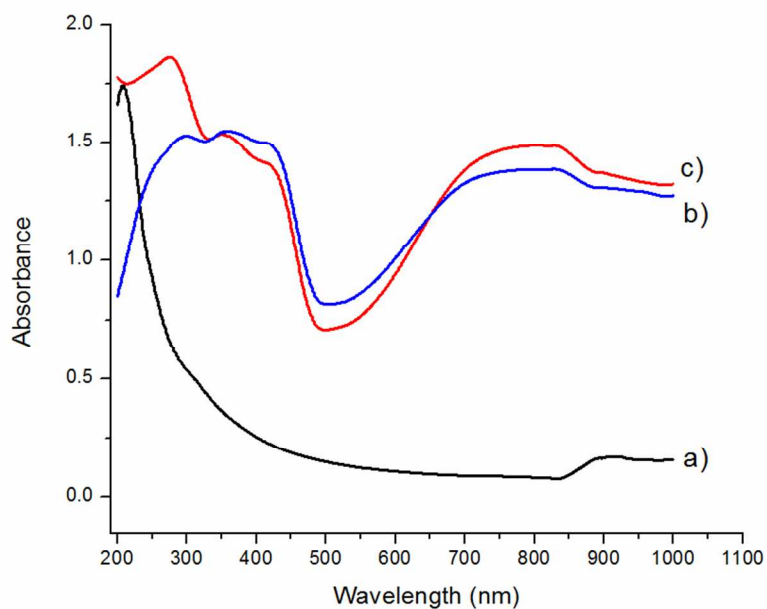


**Fig. 9** UV-vis spectra of a) GO, b) pure PANI nanofibers ( $\text{H}_2\text{SO}_4$  doped), and c) PANI-GO (PG-C).

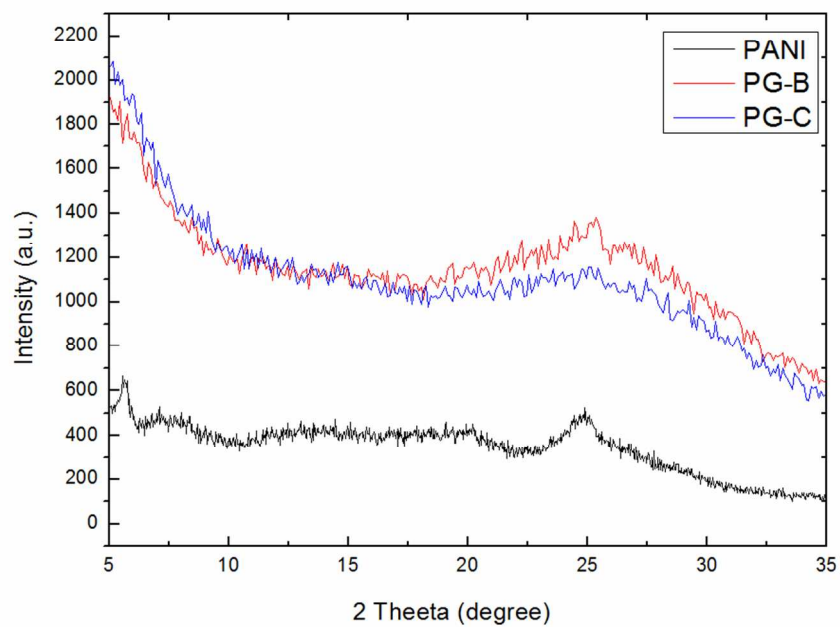


**Fig. 10** XRD patterns of pure PANI and PANI-GO.

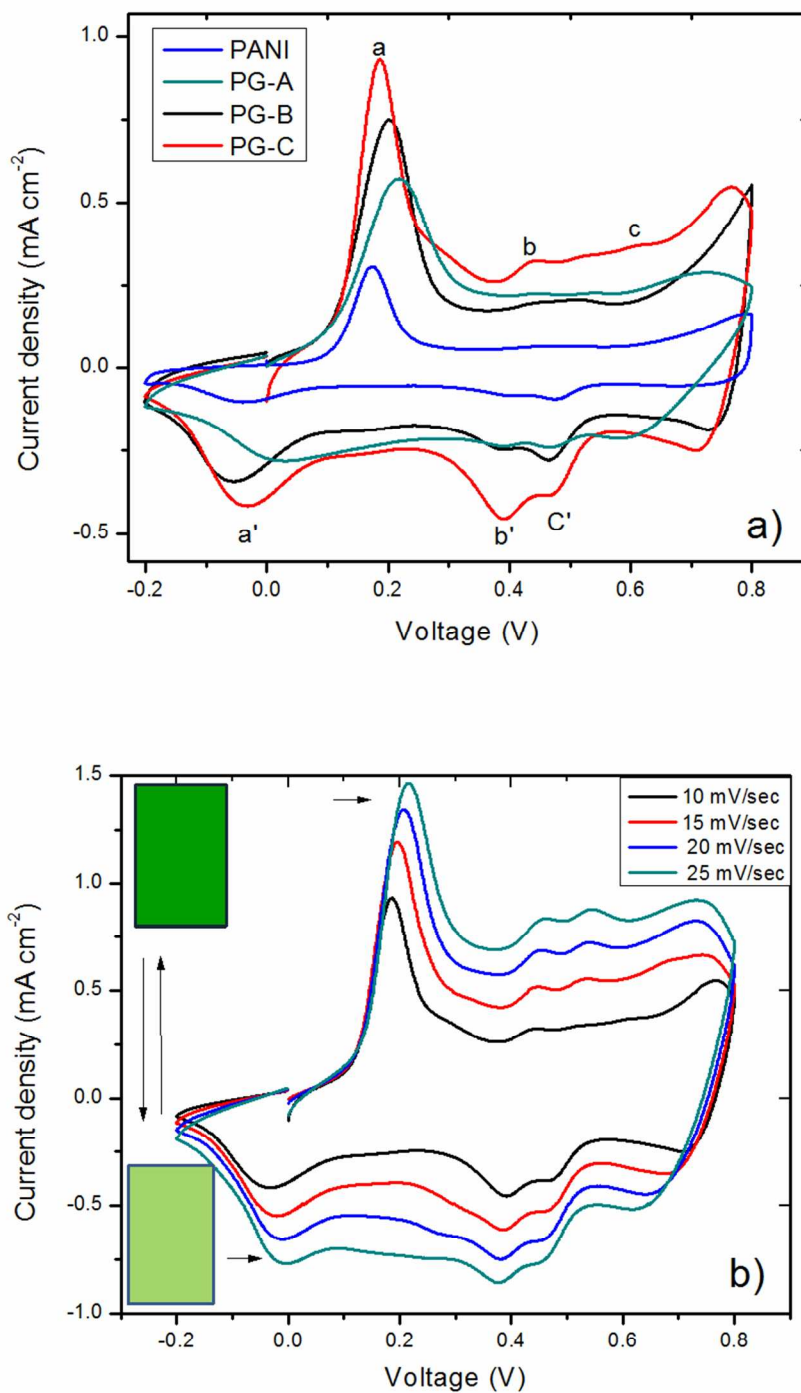


**Fig. 11** a) CV curves of PANI and PANI-GO films at scan rate of 10 mV/sec in 1 mol L<sup>-1</sup> H<sub>2</sub>SO<sub>4</sub> aqueous solution, and b) CV curves of PG-C at different scan rates, (Note: the schematic diagram in Fig b) the dark and light green color box representing the electrochromic behavior of PANI-GO film).

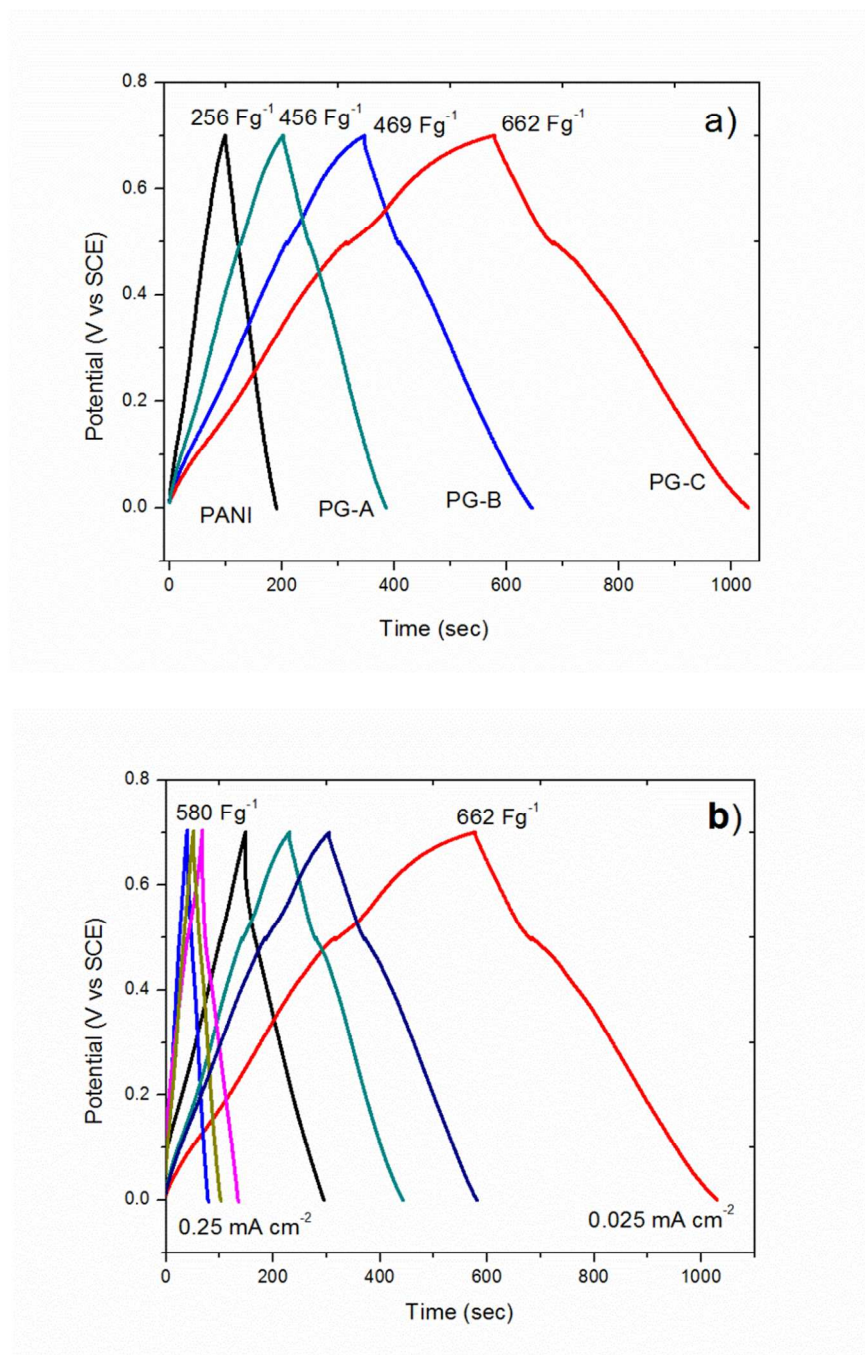


**Fig. 12** a) Galvanostatic charge-discharge curves of pure PANI and PANI-GO thin film electrodes at current density of  $0.025 \text{ mA cm}^{-2}$  within a potential window of 0 - 0.7 V in  $1 \text{ mol L}^{-1} \text{ H}_2\text{SO}_4$ , and b) Charge-discharge curves of PG-C thin film electrode at different current densities in  $1 \text{ mol L}^{-1} \text{ H}_2\text{SO}_4$ .

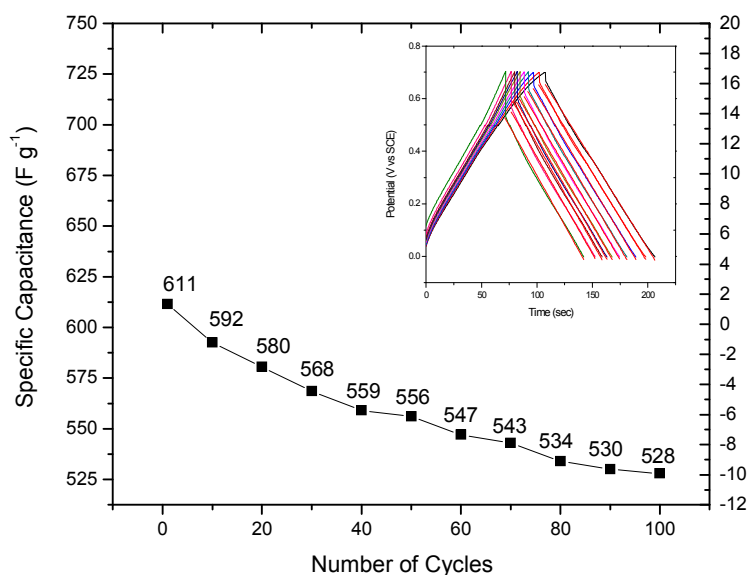


**Fig. 13** Charge-discharge cyclic performance of PG-C thin film electrode at current density of  $0.1 \text{ mA cm}^{-2}$  in  $1 \text{ mol L}^{-1} \text{ H}_2\text{SO}_4$  (Inset: charge-discharge curves of 100 cycles, each one contain ten cycles).

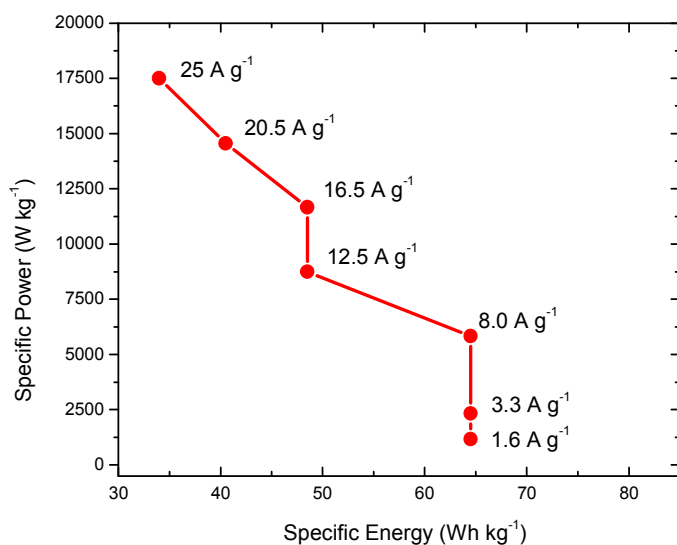


**Fig. 14** Ragone plot of specific energy vs. specific power at different specific current.

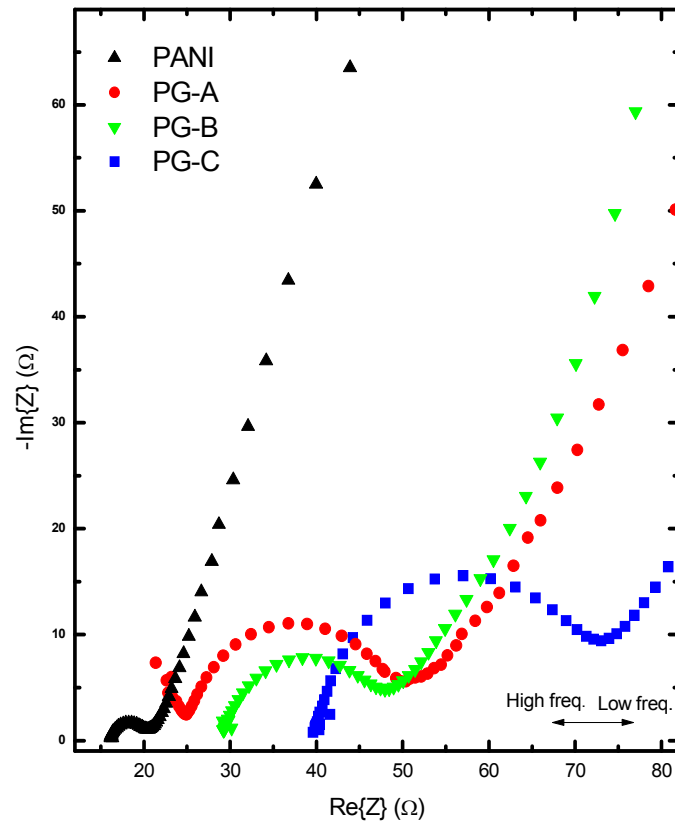


**Fig. 15** Nyquist plots for pure PANI and PANI-GO (▲ PANI, ● PG-A, ▼ PG-B, ■ PG-C)